RSC Advances

ROYAL SOCIETY OF CHEMISTRY

www.rsc.org/advances

RSC Advances

RSCPublishing

ARTICLE

Cite this: DOI: 10.1039/x0xx00000x

Non-monotonous Dependence of the Electrical Conductivity and Chemical Stability of Graphene Freestanding Film on the Degree of Reduction

Yun Kyung Jo,† In Young Kim,† Su-jin Kim, Su In Shin, Ara Go, Youngmi Lee,* and Seong-Ju Hwang*

Received 00th January 2012,
Accepted 00th January 2012

DOI: 10.1039/x0xx00000x

www.rsc.org/

The surface morphology, electrical conductivity, and chemical stability of freestanding graphene film can be effectively tailored by controlled reduction of graphene oxide (G-O) precursor. The elastic freestanding graphene films with different degree of reduction can be fabricated by vacuum-assisted filtration of reduced graphene oxide (rG-O) nanosheets prepared with different reduction time. The surface morphology and crystal structure of the resulting rG-O films can be tuned with the change of reduction condition. Of prime importance is that these graphene films do not show a monotonous dependence of electrical conductivity with the concentration of oxygenated functional groups. After the short reduction time of 30 min, the electrical conductivity of the rG-O films becomes saturated with retention of considerable amount of oxygenated groups, demonstrating the rapid establishment of electron percolation paths. Interestingly this graphene film with the reduction time of 30 min displays a higher stability with respect to microwave heating than the other films, a result of the depression of microwave absorption by the increase of electrical conductivity and the reinforced dipolar interaction between restacked graphene by the presence of oxygenated functional groups. The present work highlights the importance of controlled reduction condition in tailoring the transport property, surface morphology, and chemical stability of the rG-O freestanding films.

1. Introduction

Graphene, a two-dimensional (2D) monolayer of honeycomb carbon array, attracts intense research activities because of its unique physicochemical properties such as high electrical and thermal conductivities, great mechanical strength, and inherent flexibility.[1–3] The reduction of graphene oxide (G-O) precursor yields chemically-prepared graphene, i.e. reduced graphene oxide (rG-O).[4] Of prime importance is that the elastic graphene films can be easily fabricated by a simple vacuum-assisted filtration of the resulting rG-O colloids.[5,6] The facile preparation of freestanding graphene films widens the application fields of the graphene materials. These graphene-based materials boast excellent functionalities in many applications such as energy storage and conversion (supercapacitors, batteries, fuel cells and solar cells), field-effect transistors, biosensors and delivery vectors, gas permeable membranes, and antibacterial matrix.[7–10] Many of these functionalities of graphene rely on its high electrical conductivity and its wide surface area having oxygenated functional groups.[11-16] The electrical transport and surface property of the graphene materials are supposed to have profound influence on their application as electrodes, antibacterial matrix, catalysts, sensors, etc.[17–19] In the course of the chemical synthesis of graphene, the fine control of the reduction condition can provide an effective way not only to change the concentration and type of oxygenated functional groups of the rG-O materials but also to tailor their physicochemical properties including electrical conductivity, band gap, and surface wettability.[20-27] Generally the presence of oxygenated group is considered to degrade the electrical conductivity of the rG-O.[20] Hence, a strong reduction condition is recommended for preparing highly conductive graphene materials.[20] There is however no clear experimental evidence about the relationship between the concentration of surface functional groups and electrical conductivity of the rG-O films. In contrast to the electrical conductivity, the chemical interaction between graphene nanosheets would be enhanced by the presence of surface functional groups, thus leading to the improvement of the chemical stability of rG-O films. The content of the surface functional groups of the rG-O nanosheets is also expected to alter the surface morphology of the restacked graphene films affecting their functionalities such as catalytic and antibacterial activity.[5] Thus, for the optimization of the functionalities of these materials, it is fairly important to understand the effect of oxygenation degree on the surface morphology, electron transport property, and stability of the rG-

O films. However there is no systematic study about the effects of reduction condition on the chemical stability and surface structure of the rG-O films.

Here we report the effects of the controlled reduction of G-O precursor on the chemical bonding, electrical conductivity, surface structure, and chemical stability of the resulting rG-O films. A series of rG-O freestanding films with different degrees of oxygenation are fabricated by vacuum-assisted filtration of the rG-O materials synthesized by chemically reducing G-O under finely-controlled condition. The rG-O films with the reduction times of 7, 15, 30, and 60 min are referred to as rG-O1, rG-O2, rG-O3, and rG-O4, respectively. The chemical bonding nature, electrical conductivity, and chemical stability of these rG-O films are systematically investigated to probe how the degree of oxygenation affects the physicochemical properties of the rG-O materials.

2. Experimental

2.1 Synthesis.

The suspension of G-O was synthesized by a modified Hummers method. Briefly, 100 mg of natural graphite was mixed with 50 mL concentrated H_2SO_4 in a flask and then 500 mg of $KMnO_4$ was added.[4] After addition of $KMnO_4$, the reaction was done at 35 ℃ for 2 h under stirring. Excess distilled water (50 mL) was added to the flask (placed in an ice bath) and then more water (100 mL) was slowly added under stirring for 1 h. Hydrogen peroxide (30wt% in water, Sigma-Aldrich) was then added to the mixture until no further gas evolution was observed. The reaction proceeded for 2 h under stirring. The final suspension was filtered, washed with HCl (10% in water), and dried at room temperature under vacuum for 24 h. The colloidal suspension of G-O nanosheets (200 mL) was reduced with 35 wt% hydrazine (200 μL) and 28 wt% ammonia solution (1400 μL) at ~85 ℃ for various time intervals (7–90 min). The freestanding films of rG-O and G-O were fabricated by the vacuum-assisted filtration of the obtained rG-O and G-O suspensions at room temperature. To keep the film thickness nearly the same, much care was taken by controlling the concentration and volume of colloidal suspension; 20 ml of G-O suspension (0.05wt%) and 40 ml of rG-O suspension (0.025wt%) were used for the fabrication of G-O and rG-O films, respectively.

2.2 Characterization.

The crystal structure of the present graphene films was examined by powder X-ray diffraction (XRD, Rigaku D/Max-2000/PC, Cu Kα radiation). The morphology and thickness of the present freestanding films were probed with field emission-scanning electron microscopy (FE-SEM, Jeol JSM-6700F) (see Fig. S1 of *Supporting Information*). The chemical bonding of the present graphene materials was examined with micro-Raman spectroscopy with JY LabRam HR spectrometer using an excitation wavelength of 514.5 nm. XPS data were recorded with a PHI 5100 Perkin-Elmer spectrometer. The X-ray photoelectron spectroscopy (XPS) machine that was used adopted a twin source of X-ray beams, leading to the wide spreading of the X-ray beam and the minimization of the charging effect. In addition, all of the present XPS data were collected from a thin layer of the sample loaded on highly conductive copper foil, which suppressed the accumulation of charge during the measurement. Furthermore, any possible shift of the XPS peak caused by the charging effect was calibrated by referencing it to the C 1s peak at 248.8 eV. The variation of the electrical conductivity of graphene materials upon the change of reduction condition was probed by measuring the sheet resistance of the freestanding films of rG-O and G-O with four-point probe measurement system (Advanced instrument tech. CMT-SERIES).

3. Results and discussion

The freestanding films of rG-O1, rG-O2, rG-O3, rG-O4, and G-O are successfully fabricated by vacuum-assisted filtration of the corresponding colloidal suspensions through an Anodisc membrane filter. As can be seen clearly from Fig. 1, all the present freestanding films composed of restacked graphene nanosheets show high elasticity regardless of reduction time.

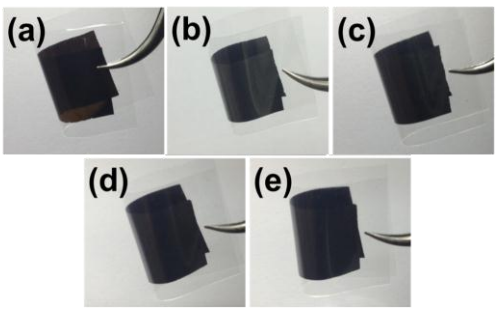

Fig. 1. Side-view photo images (in bending condition) of the restacked freestanding films of (a) G-O, (b) rG-O1, (c) rG-O2, (d) rG-O3, (e) rG-O4.

The crystal structure and morphology of the restacked freestanding graphene films are examined with XRD and FE-SEM techniques. As shown in the XRD patterns (the left panel of Fig. 2), the G-O film shows the (*002*) reflection of graphene oxide phase at $2\theta = 9.4°$, indicating the layer-by-layer-ordering the exfoliated rG-O nanosheets. The extension of reduction time leads to the shift of this peak toward high angle region with the depression of intensity, indicating the removal of surface oxygenated groups of rG-O. In comparison with powdery graphene nanosheets restored by freeze-drying process, the corresponding freestanding films commonly show stronger XRD peak intensity and higher crystallinity (see Fig. S2 of *Supporting Information*). This finding clearly demonstrates the enhanced ordering of the layer-by-layer-stacked structure of graphene nanosheets during the vacuum-assisted filtration.

As illustrated in the FE-SEM images of the right panel of Fig. 2, all the present films show wavy surface formed by the vacuum-assisted filtration process. In the case of the heavily-reduced rG-O4 film, the partial agglomeration of graphene nanosheets distinctly occurs, which is attributable to the enhanced π–π interaction of heavily-reduced rG-O nanosheets.

In fact, an agglomeration of colloidal graphene nanosheets is observed for the colloidal suspension of this heavily-reduced rG-O4 nanosheets, since the extended reduction of the G-O precursor results in the remarkable enhancement of π–π interaction. The FE-SEM analysis for the agglomerated particles restored from the rG-O4 colloid clearly demonstrates that these particles are composed by the stacked graphene nanosheets. The lateral size of these agglomerated particles matches well with those of the agglomerated particles in the freestanding rG-O4 film (see Fig. S3 of *Supporting Information*). This finding allows us to conclude that the agglomerated domains of the rG-O4 films correspond to the agglomerated graphene particles existing in the precursor rG-O4 colloidal suspension.

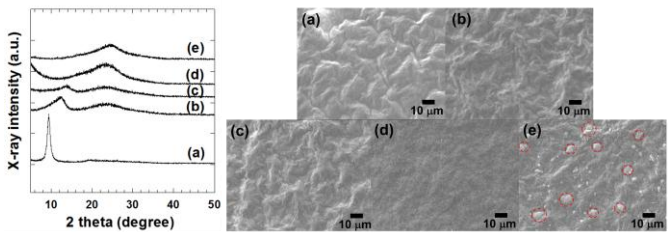

Fig. 2. (Left) XRD patterns and (right) FE-SEM images of the restacked freestanding films of (a) G-O, (b) rG-O1, (c) rG-O2, (d) rG-O3, and (e) rG-O4. In the SEM image (e), the red circles denote the agglomerated domains of graphene nanosheets.

The dependence of the concentrations of the oxygenated groups of the rG-O on the reduction time is further evidenced by micro-Raman spectroscopy, see Fig. 3. As the reduction time increases, the intensity ratio of the D/G peaks ($I_{(D)}/I_{(G)}$), a sensitive measure for the structural defects of graphene nanosheets,[28] becomes smaller (namely, D/G = 1.40, 1.39, 1.25, 1.12, and 1.10, respectively, for G-O, rG-O1, rG-O2, rG-O3, and rG-O4). This confirms a gradual curing of surface defects with increasing the reduction time.[29] After the reduction and resulting restoration of the aromaticity of the graphene lattice, a significantly decrease of $I_{(D)}/I_{(G)}$ is observed. The reduction of $I_{(D)}/I_{(G)}$ can be regarded as an indication of 'graphitization', which is related to the degree of recovery for sp^2 carbon bonds in graphitic structure.[30,31]

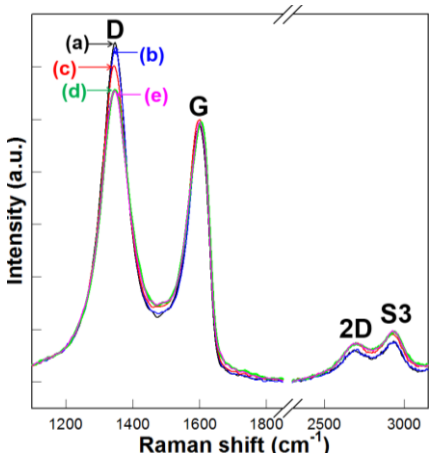

Fig. 3. Micro-Raman spectra of the exfoliated nanosheets of (a) G-O (black line), (b) rG-O1 (blue line), (c) rG-O2 (red line), (d) rG-O3 (green line), and (e) rG-O4 (pink line).

All the materials under investigation show both the 2D and S3 peaks at ~2680 and ~2940 cm^{-1}, respectively, which are assigned as the combination of defect-activated phonons.[28,32] The $I_{(2D)}/I_{(G)}$ ratios of all the present rG-O samples are estimated to be ~0.12–0.15, indicating the stacking of a few graphene layers.[28,32] The intensity of 2D peak is higher for the present rG-O materials than for the precursor G-O, confirming the graphitization of G-O upon the reduction.[33]

The evolution of the surface nature of the rG-O materials upon the change of reduction time is examined by XPS. XPS is one of the most widely used tools to determine the concentration of functional groups of nanostructured carbon-based materials. Carbon atoms in these materials possess different binding energies reflecting their chemical environments. As shown in Fig. 4, the C 1s XPS features of the present materials can be resolved into three components corresponding to the carbon atoms in different oxygen-containing functional groups: (i) the non-oxygenated sp^2 carbon (C–C, ~284.7 eV), (ii) the (epoxy+ether) group on the surface of graphene sheets (C–O–C, ~286.5 eV), and (iii) the carboxylate carbon on the edge of graphene sheets (H–O–C=O, ~289.0 eV).[34] The precursor G-O displays the highest amount of the oxygen-containing groups with (ii) + (iii) = 48.1%, see Fig. 4 and Table S1 of *Supporting Information*. The amounts of these oxygen-containing groups in rG-O1, rG-O2, rG-O3, and rG-O4 are 42.8, 37.5, 24.6, and 13.4%, respectively, showing a gradual removal of oxygenated group with increasing the reduction time.

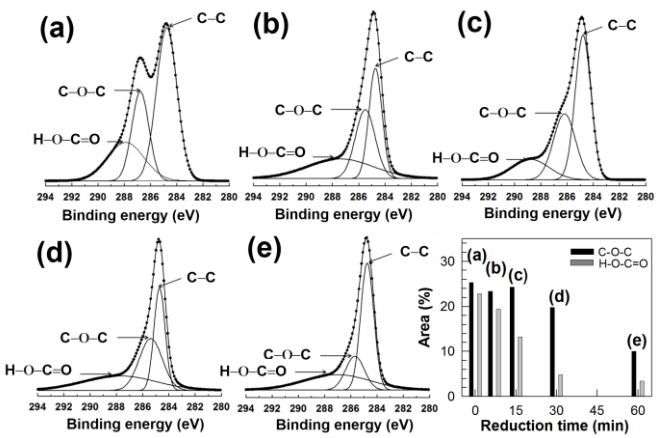

Fig. 4. (Left) C 1s XPS spectra and (bottom-right) the relative concentration plot of the functional groups for the exfoliated nanosheets of (a) G-O, (b) rG-O1, (c) rG-O2, (d) rG-O3, and (e) rG-O4.

A closer inspection for Fig. 4 reveals that the carboxyl groups are reduced prior to the (epoxy+ether) groups, indicating the poor stability of carboxyl group for chemical reduction.[35] As a consequence of the preferred reduction of carboxyl group, the ratio of {[epoxy]+[ether]}/[carboxyl] can be maximized for the rG-O3 nanosheet prepared by the

reduction for 30 min; the {[epoxy]+[ether]}/[carboxyl] ratios in G-O, rG-O1, rG-O2, rG-O3, and rG-O4 are 1.1, 1.2, 1.8, 4.1, and 2.9, respectively. This result clearly demonstrates the usefulness of the reduction time as a critical factor for controlling the nature and concentration of the oxygenated groups of the rG-O nanosheets.

The dependence of the electrical conductivity of the restacked freestanding rG-O films on the reduction time is monitored by four-point probe measurements. The electrical conductivity of the present freestanding films is calculated from the measured sheet resistance. The relationship among the sheet resistance (R_s), electrical resistivity (ρ), and electrical conductivity (σ) are given as follows:

$$\rho = R_s \times l \quad (1)$$

$$\sigma = 1 / \rho \quad (2)$$

where l is the thickness of the film. The thickness of all the obtained rG-O and G-O films are obtained from the cross-sectional FE-SEM analysis, as presented in Fig. S1 of *Supporting Information*. As plotted in Fig. 5, the electrical resistivity of the rG-O film is lowered with increasing the reduction time t. The electrical resistivity reduces quickly with increasing t until t = 30 min, but decreases slowly when t > 30 min. The reduction for t > 60 min induces no significant decrease in the electrical resistivity. This observation does not coincide with widely-accepted expectation that the conductivity of rG-O material would be proportional to the degree of reduction.

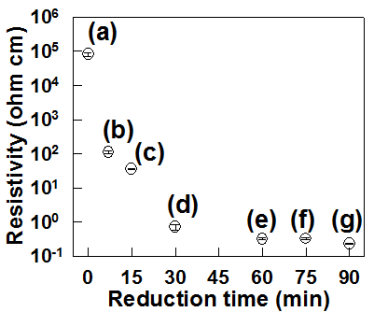

Fig. 5. The electrical resistivity of the restacked freestanding films of (a) G-O, (b) rG-O1, (c) rG-O2, (d) rG-O3, (e) rG-O4 and the heavily-reduced rG-O films prepared by the extended reduction for (f) 75 and (g) 90 min.

Actually, Chung et al. reported that solvothermally-reduced graphene oxides show an inverse correlation between reduction time and electrical resistivity, which is not consistent with the present result.[20] The observed discrepancy between the two works might be attributable to the fact that the chemical reduction with hydrazine is more efficient than the solvothermal reduction employed by Chung et al.[20] The observed rapid saturation of conductivity strongly suggests that a large number of electron percolation paths are established within 30 min of the reduction. The observed saturation of electrical conductivity is in good agreement with the theoretical prediction about the rapid formation of electrical percolation paths.[36,37] Additionally, the present finding underscores that the reduction time of 30 min is optimal for improving the electrical conductivity of rG-O with minimal loss of the surface functional groups and increasing the ratio of {[epoxy]+[ether]}/[carboxyl].

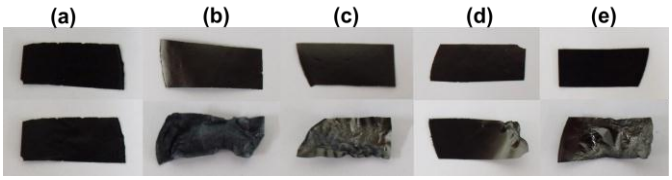

Fig. 6. Photoimages of the restacked freestanding films of (a) G-O, (b) rG-O1, (c) rG-O2, (d) rG-O3, (e) rG-O4 (top) before and (bottom) after microwave heating.

Currently microwave absorption materials with low density and low cost attract intense research interest because of their important role in many electronic devices for industry and military uses. Graphene material can be one of the promising candidates as efficient microwave absorbers. Since the adsorption of microwave might increase the local temperature of graphene nanosheet and thus induce the significant deformation of its morphology, a relationship between the degree of reduction and morphological stability of graphene under microwave irradiation is a fairly important issue for its use as microwave absorber. The effect of controlled reduction on the stability of freestanding graphene films is probed by monitoring the morphological change after the loading of microwave heating (frequency ~ 2 GHz). The photoimages of the present rG-O films subjected to are presented in Fig. 6, as compared with that of the pure G-O film. The pure G-O film does not show any significant morphological change after the microwave treatment, underscoring the high morphological stability of this material. This result strongly suggests that a stronger dipole interaction between restacked G-O nanosheets compared with van der Waals interaction of the rG-O nanosheets improves the stability of the restacked freestanding film. Conversely, all the present rG-O films suffer from considerably severe swelling and destruction after the microwave heating, which is attributable to the weakening of interaction between the restacked rG-O nanosheets due to the removal of polar functional groups. Among the present rG-O films, the rG-O3 film displays the highest stability against microwave heating. It is well-known that the increase of electrical conductivity depresses the absorption of microwave. Since this rG-O3 film possesses higher electrical conductivity than the rG-O1 and rG-O2 films, the resulting depression of microwave absorption is responsible for the higher stability of the rG-O3 film. While the rG-O4 shows similar electrical conductivity to the rG-O3, the former possesses a lower stability than the latter. As can be seen from the right panel of Fig. 2, the agglomerated particles in the precursor rG-O4 colloidal suspension is embedded in the rG-O4 films. This creates the stacking disorder of graphene nanosheets in the rG-O4 film, leading to the lowering of film stability. Such a disorder of the stacking structure is responsible for the observed lower stability of the rG-O4 film than the rG-O3 film.

4. Conclusion

In this work, the chemical bonding nature and physicochemical properties of the rG-O freestanding films can be easily tailored by a controlled reduction of the G-O precursor. The surface morphology and crystal structure of the elastic freestanding rG-O films are also tailorable with the change of reduction condition. The electrical conductivity of these films shows saturation within a short period of reduction time of 30 min. This reduction time of 30 min is much shorter than the widely-used elongated reduction time (>1 h) for preparing highly conductive rG-O nanosheets. This finding strongly suggests that the elongated reduction of G-O for longer than 30 min is not required for obtaining highly conductive rG-O nanosheets. The reduction time of 30 min is also found effective in improving the stability of the rG-O films with respect to microwave treatment. This result is interpreted as a result of the significant depression of the microwave adsorption with the tolerable weakening of the dipolar interaction between the restacked graphene nanosheets in the rG-O3 material. The present work underscores the importance of the controlled oxygenation of rG-O materials as a powerful tool not only to tailor their electrical conductivity and chemical bonding nature but also to optimize the surface morphology and chemical stability of the freestanding rG-O films.

Acknowledgements

This research is supported by the Core Technology of Materials Research and Development Program of the Korea Ministry of Intelligence and Economy (grant No. 10041232) and by National Research Foundation of Korea Grant funded by the Korean Government (2010-0001485). The authors thank to Prof. M. -H. Whangbo (North Carolina State University), Prof. J. S. Kim (Ewha Womans University), and Prof. S. H. Yoon (Ewha Womans University) for valuable discussion.

Notes and references

† These authors make equal contribution to this work.

Department of Chemistry and Nanoscience, College of Natural Sciences, Ewha Womans University, Seoul 120-750, Korea
Fax: (+82) 2-3277-3419
E-mail: hwangsju@ewha.ac.kr, youngmilee@ewha.ac.kr

Electronic Supplementary Information (ESI) available: Results of XPS deconvolution analysis for rG-O1, rG-O2, rG-O3, rG-O4, and G-O. Cross-sectional FE-SEM images of the restacked rG-O freestanding films. Powder XRD patterns of the freeze-dried rG-O nanosheets and the corresponding restacked freestanding films. Photoimage and FE-SEM image of the agglomerated particles restored from the rG-O4 colloid.

See DOI: 10.1039/b000000x/

1 K. S. Novosolev, A. K. Geim, S. V. Morozov, D. Jiang, Y. Zhang, S. V. Dubonos, I. V. Grigorieva, A. A. Firsov, *Science* 2004, **306**, 666.
2 R. Grantab, V. B. Shenoy, R. S. Ruoff, *Science* 2010, **330**, 946.
3 D. Wei, H. Zhang, L. Huang, B. Wu, J. Chen, G. Yu, *J. Am. Chem. Soc.* 2009, **131**, 11147.
4 W. S. Hummers, R. E. Offeman, *J. Am. Chem. Soc.* 1958, **80**, 1339.
5 I. Y. Kim, S. Park, H. Kim, S. Park, R. Ruoff, S. -J. Hwang, *Adv. Funct. Mater.* 2014, **24**, 2288.
6 C. Li, J. Adamcik, R. Mezzenga, *Nat. Nanotechnol*. 2012, **7**, 421.
7 M. D. Stoller, S. Murali, N. Quarles, Y. Zhu, J. R. Potts, X. Zhu, H. W. Ha, R. S. Ruoff, *Phys. Chem. Chem. Phys*. 2012, **14**, 3388.
8 Y. Xue, D. Yu, L. Dai, R. Wang, D. Li, A. Roy, F. Lu, H. Chen, Y. Liu, J. Qu, *Phys. Chem. Chem. Phys*. 2013, **15**, 12220.
9 Y. R. Lee, I. Y. Kim, T. W. Kim, K. M. Lee, S. -J. Hwang, *Chem. Eur. J.* 2012, **18**, 2263.
10 C. Lu, H. Yang, C. Zhu, X. Chen, G. Chen, *Angew. Chem*. 2009, **121**, 4879; *Angew. Chem. Int. Ed*. 2009, **48**, 4785.
11 S. Stankovich, D. A. Dikin, G. H. B. Dommett, K. M. Kohlhaas, E. J. Zimney, E. A. Stach, R. D. Piner, S. T. Nguyn, R. S. Ruoff, *Nature* 2006, **442**, 282.
12 A. A. Balandin, S. Ghosh, W. Bao, I. Calizo, D. Teweldebrhan, F. Miao, C. N. Lau, *Nano Lett*. 2008, **8**, 902.
13 G. Xiong, C. Meng, R. G. Reifenberger, P. P. Irazoqui, T. S. Fisher, *Adv. Energy. Mater.* 2014, **4**, 1300515.
14 G. Xiong, K.P.S.S. Hembram, D. N. Zakharov, R.G. Reifenberger, T. S. Fisher, *Diamond Relat. Mater.* 2012, **27-28**, 1.
15 G. Xiong, C. Meng, R. G. Reifenberger, P. P. Irazoqui,T, S. Fisher, *Electroanal*. 2014, **26**, 30.
16 G. Xiong, K.P.S.S. Hembram, R.G. Reifenberger, T. S. Fisher, *J. Power Sources* 2013, **227**, 254.
17 M. Kim, Y. Hwang, K. Min, J. Kim, *Phys. Chem. Chem. Phys*. 2013, **15**, 15602.
18 M. Mishra, R. K. Joshi, S. Ojha, D. Janjilal, T. J. Mohanty, *Phys. Chem. C* 2013, **117**, 19746.
19 S. Myung, A. Solanki, C. Kim, J. Park, K. S. Kim, K. -B. Lee, *Adv. Mater*. 2011, **23**, 2221.
20 V. H. Pham, R. V. Cuing, S. H. Hur, E. Oh, E. J. Kim, E. W. Shin, J. S. Chung, *J. Mater. Chem*. 2011, **21**, 3371.
21 L. Z. Fan, J. L. Liu, R. U. Din, X. Yan, X. Qu, *Carbon* 2012, **50**, 3724.
22 S. Stankovich, D. A. Dikin, R. D. Piner, K. A. Kohlhaas, A. Kleinhammes, Y. Jia, Y. Wu, S. T. Nguyen, R. S. Ruoff, *Carbon* 2007, **45**, 1558.
23 W. Chen, L. Yan, P. R. Bangal, *Carbon* 2010, **48**, 1146.
24 D. Luo, G. Zhang, J. Liu. X. Sun, *J. Phys. Chem. C* 2011, **115**, 11327.
25 A. Mathkar, D. Tozier, P. Cox, P. Ong, C. Galande, K. Balakrishnan, A. L. M. Reddy, P. M. Ajayan, *J. Phys. Chem. Lett*. 2012, **3**, 986.
26 L. Guo, R. Q. Shao, Y. L. Zhang, H. B. Jiang, X. B. Li, S. Y. Xie, B. B. Xu, Q. D. Chen, J. E. Song, H. B. Sun, *J. Phys. Chem. C* 2012, **116**, 3594.
27 J. N. Wang, R. Q. Shao, Y. L. Zhang, L. Guo, H. B. Jiang, D. X. Lu, H. B. Sun, *Chem. Asian J*. 2012, **7**, 301.
28 A. C. Ferrari, J. C. Meyer, V. Scardaci, C. Casiraghi, M. Lazzeri, F. Mauri, S. Piscanec, D. Jiang, K. S. Novoselov, S. Roth, A. K. Geim, *Phys. Rev. Lett*. 2006, **97**, 187401.
29 J. I. Paredes, S. Villar-Rodil, P. Solis-Fernandez, A. Martinez-Alonso, J. M. Tarascon, *Langmuir* 2009, **30**, 5957.
30 A. C. Ferrari, J. Robertson, *Phys. Rev. B* 2000, **61**, 14095.
31 C. C. Han, J. T. Lee, H. Chang, *Chem. Mater*. 2001, **13**, 4180.
32 C. Casiraghi, S. Pisana, K. S. Novoselov, A. K. Geim, A. C. Ferrari, *Appl. Phys. Lett.* 2007, **91**, 23310891.

33 V. C. Tung, M. J. Allen, Y. Yang and R. B. Kaner, *Nat. Nanotechnol*. 2008, **4**, 25.
34 H. A. Becerril, J. Mao, Z. F. Liu, R. M. Stoltenberg, Z. N. Bao, Y. S. Chen, *ACS Nano* 2008, **3**, 463.
35 S. Pei, H. M. Cheng, *Carbon* 2012, **50**, 3210.
36 D. Stauffer, *Introduction to Percolation Theory*, Taylor & Francis, London, 1985.
37 J. Sato, H. Kato, M. Kimura, K. Fukuda, W. Sugimoto, *Langmuir* 2010, **26**, 18049.

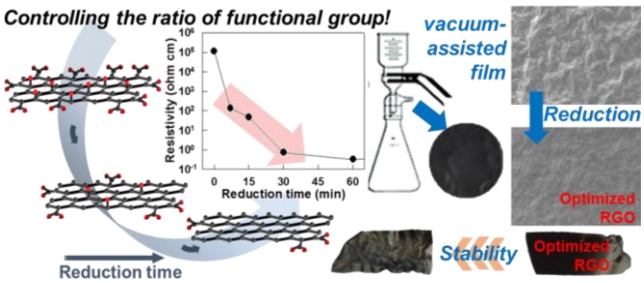

The controlled oxygenation of rG-O nanosheet is quite effective in controlling the chemical bonding nature and surface morphology of graphene films and also in optimizing their electrical conductivity and stability.